Ultrasonics 54 (2014) 621–631

Contents lists available at ScienceDirect

Ultrasonics

journal homepage: www.elsevier.com/locate/ultras

Study of ultrasound stiffness imaging methods using tissue mimicking phantoms

Kavitha Manickam [a,*], Ramasubba Reddy Machireddy [a], Suresh Seshadri [b]

[a] Biomedical Engineering Group, Department of Applied Mechanics, IIT Madras, Chennai 600036, India
[b] Mediscan Systems, Chennai 600004, India

ARTICLE INFO

Article history:
Received 11 June 2013
Received in revised form 23 August 2013
Accepted 30 August 2013
Available online 12 September 2013

Keywords:
Ultrasound stiffness imaging
Tissue mimicking phantom
Acoustic characterization
Elastic characterization
Elastography

ABSTRACT

A pilot study was carried out to investigate the performance of ultrasound stiffness imaging methods namely Ultrasound Elastography Imaging (UEI) and Acoustic Radiation Force Impulse (ARFI) Imaging. Specifically their potential for characterizing different classes of solid mass lesions was analyzed using agar based tissue mimicking phantoms. Composite tissue mimicking phantom was prepared with embedded inclusions of varying stiffness from 50 kPa to 450 kPa to represent different stages of cancer. Acoustic properties such as sound speed, attenuation coefficient and acoustic impedance were characterized by pulse echo ultrasound test at 5 MHz frequency and they are ranged from (1564 ± 88 to 1671 ± 124 m/s), (0.6915 ± 0.123 to 0.8268 ± 0.755 db cm^{-1} MHz^{-1}) and ($1.61 \times 10^6 \pm 0.127$ to $1.76 \times 10^6 \pm 0.045$ kg m^{-2} s^{-1}) respectively. The elastic property Young's Modulus of the prepared samples was measured by conducting quasi static uni axial compression test under a strain rate of 0.5 mm/min upto 10 % strain, and the values are from 50 kPa to 450 kPa for a variation of agar concentration from 1.7% to 6.6% by weight. The composite phantoms were imaged by *Siemens Acuson S2000 (Siemens, Erlangen, Germany)* machine using linear array transducer 9L4 at 8 MHz frequency; strain and displacement images were collected by UEI and ARFI. Shear wave velocity 4.43 ± 0.35 m/s was also measured for high modulus contrast (18 dB) inclusion and X.XX m/s was found for all other inclusions. The images were pre processed and parameters such as Contrast Transfer Efficiency and lateral image profile were computed and reported. The results indicate that both ARFI and UEI represent the abnormalities better than conventional US B mode imaging whereas UEI enhances the underlying modulus contrast into improved strain contrast. The results are corroborated with literature and also with clinical patient images.

1. Introduction

Ultrasound B-mode imaging is a popular and most widely used method for imaging breast, thyroid, prostate and human abdominal organs like kidney, spleen and liver. Even though it is used as a screening tool in cancer diagnosis, it is poor at distinguishing cancerous tissue from soft tissue. Basically there are two types of cancer tissue namely benign and malignant depending on whether or not they can spread by invasion and metastasis. Benign lesions are those that cannot spread out by invasion. They grow only locally and they can be cured by suitable therapy where as malignant tumor invades neighboring cells, enter into blood vessels, lymphatic system and metastasize to different sites. For distinguishing benign and malignant lesions, conventional ultrasound techniques use B-mode image shape features like lesion margin irregularity, shadowing, microlobulation and wider than taller orientation. However these features are often found to be overlapping, which decreases the reliability of B-mode in classification of lesions [1]. This leads to invasive biopsies to confirm the presence of cancer which causes patient discomfort and unnecessary anxiety. On the other hand, pathological cancerous changes of tissues are highly correlated with changes in stiffness [2]. Abnormalities such as benign and malignant cancer lesions could be identified based on their stiffness properties; benign tumors are generally around 2–3 times stiffer than normal tissues and deform more for an applied compression. But malignant tumors are harder than surrounding tissues and show less deformation. Thus they can be distinguished by stiffness contrast than acoustic contrast and this property is used in stiffness imaging. In recent decades, there has been an increasing need in assessing the stiffness properties like Young's modulus E and shear modulus G of tissues. In isotropic materials, the ratio of longitudinal deformation (strain) in response to an applied longitudinal force (stress) is known as Young's modulus (E) of elasticity. The shear modulus (G) relates transverse strain to transverse stress. A number of stiffness imaging modalities are being developed and they are based on applying a mechanical excitation to tissues of interest and measuring tissue deformation.

* Corresponding author. Tel.: +91 9444023139.
E-mail address: kavitharunkumar@gmail.com (K. Manickam).

0041-624X/$ - see front matter © 2013 Elsevier B.V. All rights reserved.
http://dx.doi.org/10.1016/j.ultras.2013.08.018

The measured deformation can be displayed directly as an image or strain is computed and displayed as a grey scale map known as elastogram [3].

Stiffness imaging methods are categorized according to the source of mechanical excitation and how the local displacements are measured. Mechanical excitation may be either 'external' via probe (static or quasi static) [3], 'organic' which relies on natural movements of the body like heart beat, pulsing of blood vessels [4,5], 'dynamic' external vibration to create shear waves within the tissue of interest called as sonoelasticity [6] or locally by acoustic radiation force [7]. Stiffness imaging methods can be further classified based on the method of deformation measurement either by ultrasound [3–5], Magnetic Resonance Imaging [8] or optical methods [9]. The focus of this paper is on Ultrasound Elastography Imaging (UEI) which is based on external compression and Acoustic Radiation Force Impulse (ARFI) [10–12] imaging which is based on force generated by ultrasound.

Initial clinical results were obtained for identifying breast [13], thyroid [14,15] and liver [16] using UEI and ARFI imaging. However, issues like amount of compressive force to be applied to get repeatability in Ultrasound Elastography, image contrast representations between tumor and background, complex nature of tissue structures and data on elastic properties of normal and pathological tissues need through evaluation [17,18]. In clinical setting, Ultrasound Elastography and ARFI imaging are still not standardized as B-mode imaging in terms of instrumentation parameters like optimum gain setting, dynamic range, and depth of penetration. In order to do this, there is a need for a large database of stiffness properties of different categories of human tissue. It would be difficult to obtain tissues exhibiting malignant or benign features at will. Moreover biological tissues lose their characteristics with time when they are harvested from body. It is hence necessary to develop tissue mimicking phantoms which have identical acoustic (speed of sound, attenuation coefficient and acoustic impedance) and elastic properties (Young's modulus and shear modulus) of human soft and cancerous tissues. Tissue mimicking phantoms should be temporally stable; when they are tested diagnostically for validation and training purposes, the geometry, acoustic and elastic properties should be maintained within a tolerable range of 1–2% or it should be at least predictable [19,20]. The commonly used physical gels for tissue like phantoms are agar and gelatin [19,21] where as chemical gels are polyacrylamide [22] and polyvinyl alcohol [9]. Since physical gel phantoms are made by hydrogels, there is a chance for bacterial invasion and reduction of water content as time passes through. Proper care must be taken to avoid the desiccation of water from phantoms. Chemical gel phantoms might be more stable than physical gel phantoms [23], however physical gel phantoms are easier, safer and can be made stable for a longer duration (more than 6 months) either by adding preservatives or with suitable preconditioning. [21].

Having said all these, the objective of this work is to study the performance of UEI and ARFI imaging by quantifying how well the underlying elastic modulus contrast is represented for various categories of inclusions made in tissue mimicking phantoms. As yet, no studies have compared the performance of conventional Ultrasound B mode, UEI and ARFI in custom made tissue mimicking phantoms. The performance is evaluated by finding out the parameters namely Contrast Transfer Efficiency (CTE) and lateral image profile which is the pictorial representation of contrast distribution in image. Lateral image profile gives the degree with which the inclusion is differentiated locally from its surrounding tissue whereas Contrast Transfer Efficiency gives how well the actual contrast (elastic contrast of inclusion to background) is depicted in image. In order to achieve this, agar based homogeneous phantoms were made and their acoustical properties were characterized using pulse echo ultrasound test. Mechanical properties were measured by conducting uni axial compression test on Universal Testing Machine (UTM). Thereafter a composite phantom with embedded inclusions were prepared and stiffness parameters were imaged using *Siemens Acuson S2000 (Siemens, Erlangen, Germany)* machine. Both qualitative and quantitative results were obtained. The resultant strain images were pre-processed and parameters were extracted to assess the performance. The paper is organized as follows. In Section 2, we explain about the development of phantoms and their characterization based on measurement of acoustic and elastic properties. Then we present design, development of composite phantom and the imaging techniques. In Section 3, the results are discussed.

2. Materials and methods

2.1. Preparation of tissue mimicking phantoms

The most common tissue mimicking materials are gelatine, agar, urethane rubber, zerdine, polyvinyl alcohol and polyacrylamide. In this work, we have chosen agar as the basis of our phantom due to the following reasons.

- Agar exhibits near linear response of attenuation to frequency ($f^{1.01}$) [24].
- Change in acoustic velocity due to temperature change is less than 3 m/s [24].
- The differences in concentration of agar will give variations in stiffness (from kPa to MPa).
- Agar phantoms can be stored in distilled water for longer duration (3 months) without much change (0.5–1%) in properties due to water loss.

The components of phantom sample are agar, N-propanol and deionized water. In plain agar, ultrasound travels slowly. N-propanol was added to increase the speed of sound to be matched with human tissue (1540 m/s). Samples were made by varying concentration of agar from 2 g to 12 g [25]. Sample with 12 g was too stiff to be tested due to the brittle nature of agar at higher concentration. Hence we restricted our study on samples from 2 g to 10 g agar.

2.2. Characterization of acoustic properties

In order to perform ultrasound stiffness imaging, the prepared samples do mimic soft tissues in terms of acoustic and elastic properties. The chosen acoustic parameters are acoustic velocity, attenuation coefficient and acoustic impedance. Pulse echo method was used to measure acoustic properties. We used 5 MHz, 6 mm contact type single element transducer *(V110RM, Olympus NDT)*. The excitation and receiving pulses were controlled by a pulser receiver *(5677, Olympus NDT)* which was operated in pulse echo mode. The received echoes were digitized by a digitizer *(PXI 5122, National Instruments)* at a sampling rate of 50 MHz, acquired using virtual instrument software LabVIEW and analyzed using Matlab. The time difference between two successive received echoes (t) and the amplitudes (A1 and A2) of echoes were measured from the digitized data. The density $\rho(\mathrm{kg/m^3})$ of the material is determined as the ratio of mass to volume. The dimensions of the phantoms were measured using vernier caliper *(Mitutoyo, Japan)* and mass was measured using a digital weighing machine *(Sartorius, India)*. From these data, the acoustic parameters such as speed of sound (V), attenuation coefficient (A) and acoustic impedance (Z) were calculated for all the prepared phantom samples using standard formulae.

$$V(\mathrm{m/s}) = \frac{2d}{t} \quad (1)$$

$$A(\mathrm{dB/cm}) = \frac{1}{2d} 20log\frac{A1}{A2} \quad (2)$$

$$Z(\mathrm{kg/m^2\ s}) = \rho V \quad (3)$$

where d is the height of the sample in meters. The samples are disc shaped having 50 mm diameter and 20 mm thickness (Fig. 1). Acoustic properties were verified with 2.25 MHz, 0.25 in. transducer *(V133RM, Olympus NDT)* and 10 MHz, 0.25 in. transducer *(V537RM, Olympus NDT)*.

2.3. Characterization of elastic parameters

In this work, human soft tissue is assumed to exhibit linear elastic behavior. During imaging, compression less than 5% of strain is given to probe the mechanical properties of tissues. In this small strain range (0–5%), stress strain curves are linear and they could be approximated by Youngs Modulus using Hooke's law. Young's Modulus of the samples is measured from uni axial compression test conducted on Universal Testing Machine (UTM) *(Jinan TE, china)*. The 50 kN machine is equipped with an extensometer with 50 mm gauge length and 10 mm deformation. Load cell measures test load and deformation of the specimen is measured by extensometer. Measurements were performed after the sample reached room temperature. Samples were immersed in deionized water in order to avoid any sample desiccation. The phantom sample was made such that its height is less than twice of its diameter to avoid buckling effect. Compression test was conducted under the displacement controlled mode. The load was applied under a strain rate of 0.5 mm/min up to a maximum of 10% strain and then it was unloaded in the similar way. Typically all samples were preloaded to 1% of strain (0.7 mm). From the recorded data, stress and strain relationship of the phantom under uni axial loading was plotted and Young's modulus was calculated from the initial portion of stress strain curve.

The samples included in compression test were cylindrical in shape with 38 mm diameter and 70 mm height. The photograph of the phantom samples are shown in Fig. 1.

2.4. Composite phantom

To study the elastographic behavior of pathological regions of varying stiffness, a composite phantom was made with solid hard inclusions which are harder than the background tissue. Here we made two types of hard inclusions which are low modulus contrast inclusions (modulus ratio between inclusion and background is around 10 dB) and high modulus contrast inclusions (modulus ratio is above 10 dB) [26]. There were three inclusions namely EI_4, EI_6 and EI_8 and their elastic properties are summarized in Table 1.

These inclusions are embedded in an uniform background which resembles normal soft tissue. Phantom is having the dimensions of $14 \times 14 \times 3.5$ cm (length $\times$ width $\times$ height). Each inclusion (EI_4, EI_6 and EI_8) is of cylindrical shape having 1.5 cm diameter and 1 cm height. The plan, elevation and photograph of the composite phantom are shown in Fig. 2(a–c). This study has been done with five realizations of composite phantom and each time we took five images of each inclusion and background using UEI and ARFI imaging.

In reality, the shape of the inclusion might be anything like sphere, rectangle or any irregular shape. However, considering that most of the breast tumors can be approximated to have a cylindrical shape [1], we did not consider other shapes.

2.5. Ultrasound Elastography Imaging (UEI) technique

Ultrasound Elastography is a method of imaging mechanical properties of tissues specifically related to Young's Modulus. It is known as remote palpation and is described by Ophir et al. [3]. The basic principle of UEI involves acquiring and comparing ultrasound signals from tissues before and after a small quasi static external compression (less than 5% strain). When the body tissues are compressed, the softer parts deform more easily than the harder parts. The displacement or strain produced inside the tissue due to the compression is computed from the acquired signal based on correlation techniques and displayed as an elastogram.

Ultrasound B mode (prior to application of force) and elastograms (after compressive force) were acquired using *Siemens Acuson S2000 (Siemens, Erlangen, Germany)* machine at Mediscan Systems, Chennai. Linear array transducer *9L4* with a probe frequency of 8 MHz was used. Initially, B mode image of the region of interest (ROI) was obtained. Once the ROI was highlighted in B-mode image, a compression around 5 N was applied by pressing the probe on the phantom surface by expert radiologist. It was measured using a weighing balance placed under the phantom. Elastogram was generated by the scanner by comparing the pre-compressed and post-compressed RF signals and displayed adjacent to the B mode image. Using the aforementioned procedure, elastograms of all the three inclusions and background were obtained.

2.6. ARFI Imaging

ARFI imaging is implemented in Siemens Acuson S2000 ultrasound machine in two modes namely Virtual Touch Tissue Imaging (VTTI) and Virtual Touch Tissue Quantification (VTTQ). VTTI displays an image which has the information about displacement of lesion and its surrounding tissue whereas VTTQ provides numerical output which is the shear wave speed which is proportional

Fig. 1. Photograph of phantom samples (a) mechanical property measurement (b) acoustical property measurement.

Table 1
Concentration, Young's Modulus and true modulus ratio of the composite phantom.

Type	Agar concentration (g)	Young's Modulus (kPa)	True modulus ratio
Background	2	52	–
EI_4 (Low modulus contrast)	4	182	3.5 (10 dB)
EI_6 (High modulus contrast)	6	347	6.6 (16 dB)
EI_8 (High modulus contrast)	8	448	8.6 (18 dB)

to the stiffness of underlying tissue. Initially a B-mode image of the composite phantom was obtained and (EI_8) inclusion was highlighted as the Region Of Interest (ROI). A short duration (less than 1 ms) pulse, known as push pulse was passed through ROI which gives mechanical force. Due to this force, the agar particles of the phantom were displaced depending on their stiffness. Immediately after that, tracking pulses which are normal diagnostic ultrasound pulses were applied on ROI for certain interval. The reflected echoes were collected. Images were formed by these reflected beams and compared with the initial ROI image obtained prior to the application of push pulse. The displacements were computed and displayed as an ARFI image. The experiment was repeated for the remaining two inclusions (EI_4 and EI_6) and displacement images were obtained.

In the same machine, VTTQ was also done which is the tool for obtaining numerical value of stiffness at precise image based anatomical location. The sonographer selected the depth at which the elasticity is evaluated by placing a measuring box (ROI) of (10×5 mm) at the desired place. Then push pulse was applied for shorter duration (less than 1 ms) which is similar to VTTI. Since all the three inclusions are of solid nature, ARFI generates shear waves which propagate away from the ROI. Tracking pulses were applied to capture the displacement caused by the moving wave front of shear wave. From the captured data, velocity of shear wave which characterizes the stiffness was computed. If the ROI is a fluid medium, ARFI results in the steady motion of fluid in axial direction known as acoustic streaming. The velocity of fluid motion relates with the viscosity of the fluid. Shear wave speed and fluid motion velocity can be calculated from tissue displacements [11]. At present we have done the experiments for obtaining shear wave speed in solid masses only. Shear wave speed which is displayed in m/s, increases with stiffness. Since the mechanical excitation is guided by ultrasound B-mode imaging and done by ultrasound pulses, ARFI could be applicable for deep tissues which are not accessible to superficial compression elastography techniques.

3. Results and discussion

3.1. Elastic properties

Uni axial compression test was performed using UTM to compute Young's Modulus for samples with different agar concentration from 2 g to 10 g. By measuring the stress for several different applied strain, the stress–strain behavior of samples was characterized. Compression test was conducted upto 10% of strain. Typical stress strain curve of one sample is shown in Fig. 3(top). Young's Modulus values were calculated from initial linear region (upto 4 % of strain) of the curves using least square fit. Measurements were made for five sets of samples at three different times. The results shown in Fig. 3(bottom) are the average of the measurements and the errors are the standard deviation. The total range of elastic moduli achieved by varying the agar concentration from 2 g to 8 g is 50 kPa to 450 kPa which covers the entire range of normal and abnormal tissue stiffness [27,28]. Since the Young's Modulus of 10 g sample is 1024 kPa which is very high for human soft tissue, we excluded the sample from this study. The change in modulus from the sample mimicking normal tissue (2 g) to the samples mimicking cancerous tissue (4–8 g) is large enough to achieve the desired contrast between lesion and the surrounding tissue. In ultrasound elastography applications, the difference in elastic modulus between the lesion and the surroundings is to be of great importance than the absolute value of the modulus.

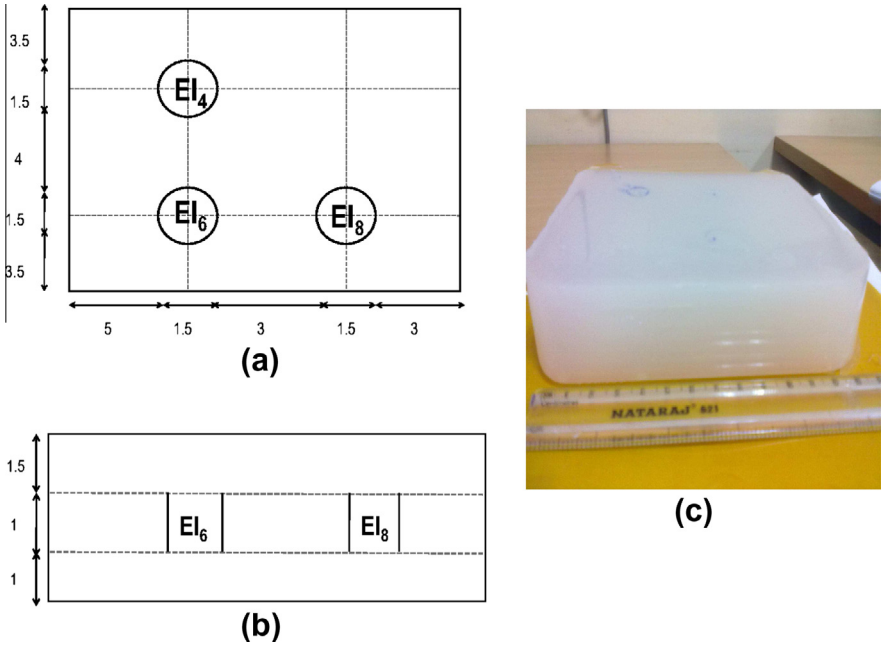

Fig. 2. (a) Plan, (b) elevation and (c) photograph of the composite phantom with inclusions of varying stiffness. All the dimensions are given in cm.

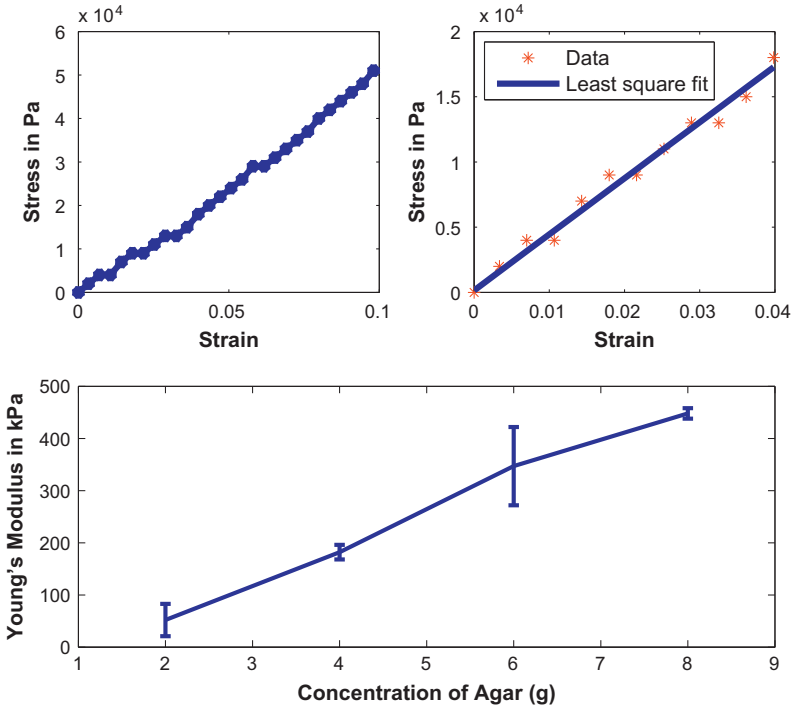

Fig. 3. (top) Stress strain characteristics of 8 g sample. Linear region is fixed at the initial portion (4% of strain) and solid line shows the least square fit. (bottom) Mean and standard deviation of Young's Modulus for various samples of agar concentration from 1.7% to 6.6 % (2–8 g).

3.2. Acoustic properties

For acoustic measurement, samples of same agar concentrations were prepared. The acoustic parameters such as sound speed, attenuation coefficient and acoustic impedance were calculated. The mean and standard deviation values are presented in Table 2 along with corresponding values for the human tissue [29,30] for comparison. The results of our samples match with the literature values.

The results were verified with 2.25 and 10 MHz transducers and the results are in the same range reported for 5 MHz shown in Table 2. Sound speed and acoustic impedance are independent of the frequency. But attenuation (db cm^{-1}) increases with increase in frequency from 2.25 to 10 MHz. Since it varies linearly for agar [24], the phantoms could be operated in the range of diagnostic frequencies (from 3- 15 MHz).

Having characterized the elastic and acoustic properties of homogeneous samples, a composite phantom was made with 3 inclusions to mimic different stages of cancer as explained in Section 2.4. Inclusions were made such that they are 3–8 times stiffer than the background.

3.3. Ultrasound Elastography Imaging (UEI)

The elastographic images (left) and ARFI displacement images (right) of the composite phantom with embedded inclusions are displayed along with ultrasound images (center) in Fig. 4(a–c) in order to make comparison. In B-mode imaging, the inclusions are seen as hyper echoic regions and they are not significantly differentiated from the background. In elastograms, dark region represents less strain or no strain where bright areas represent more strain. The grey scale bar is displayed along with the images, which shows the images have different strain components. The high modulus contrast inclusion (EI_8) exhibits no strain compared to the background and its area in image is well appreciated in black color. In case of (EI_6) inclusion, the area of inclusion is not uniformly dark and intermediate strain components are introduced, which shows the increased strain. In the case of low modulus contrast inclusion (EI_4), more amount of strain is introduced where we can not get a clear boundary at all. The elastogram of the background without any inclusion was also obtained and shown in Fig. 4(d), which does not show any specific pattern.

3.4. ARFI

ARFI VTTI images for all three types of lesions are displayed at the right side in Fig. 4(a–c). The images portray the displacement information of agar particles. Inclusion portion is highlighted for clarity. Dark region indicates less or no displacement which is interpreted as hard inclusion where brightness represents more compliance.

Table 2
Acoustic properties of the prepared samples and human tissue.

Parameters	Human tissue [29,30]	2 g Agar sample	4 g Agar sample	6 g Agar sample	8 g Agar sample
Sound speed (m/s)	1540	1564 ± 88	1581 ± 26	1571 ± 12	1671 ± 124
Attenuation coefficient (db cm^{-1} MHz^{-1})	0.7	0.8268 ± 0.755	0.6915 ± 0.123	0.7802 ± 0.003	0.7121 ± 0.2313
Acoustic impedance (kg m^{-2} s^{-1})	1.63×10^6	$1.66 \times 10^6 \pm 0.165$	$1.76 \times 10^6 \pm 0.045$	$1.61 \times 10^6 \pm 0.127$	$1.71 \times 10^6 \pm 0.012$

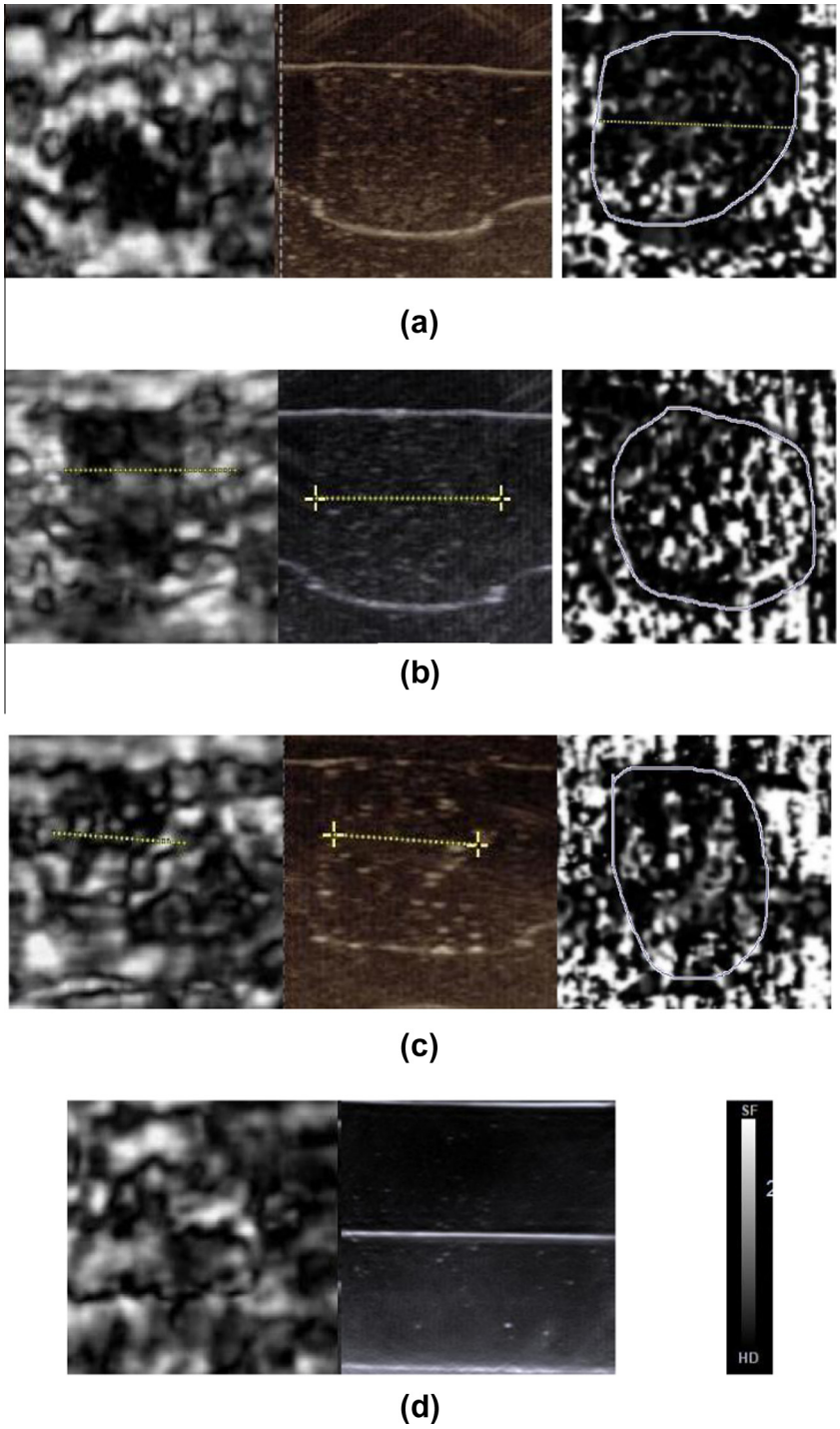

Fig. 4. (a–c) Elastogram (left side), Ultrasound B mode (center) and ARFI displacement images (right side) of the three inclusions EI_8, EI_6, EI_4 respectively and (d) shows B mode and elastogram of background. All the images are represented as per the grey color bar.

VTTQ was also performed for all the three inclusions. At each inclusion, at different sites the experiments were performed. Fig. 5 shows the resultant image for EI_8. Shear wave velocity obtained is 4.43 ± 0.35 m/s. When stiffness decreases, the shear wave velocity is expected to decrease further. We could not get proper shear wave velocity values for other types of inclusion. For the other two, scanner displayed as X.XX which means that they are not deterministic. It may be because of few inhomogeneities present in the phantom which might be added while preparation.

3.5. Performance analysis

In order to make performance comparison of US B-mode with UEI and ARFI VTTI, parameters such as Contrast Transfer Efficiency and lateral image profile were extracted from images. Prior to extraction of parameters, the images were preprocessed to eliminate speckle noise. Speckle noise is the inherent property of medical ultrasound imaging. It generally reduces image resolution and contrast. Prepared tissue mimicking phantoms could contribute to tissue like grainy structure in image. To achieve the purpose, gen-

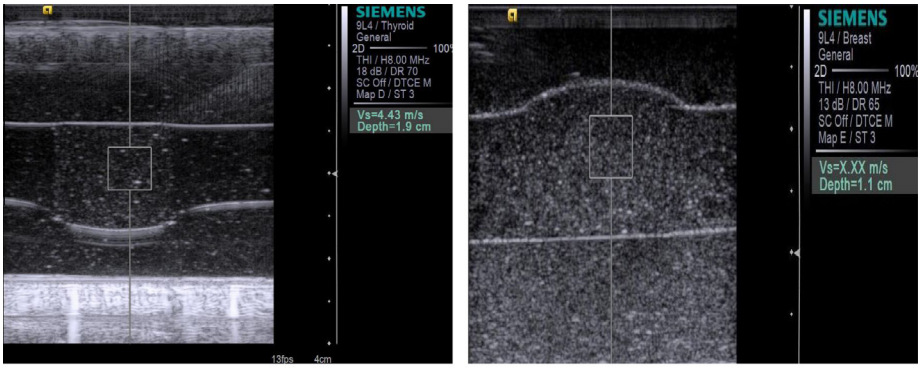

Fig. 5. Shear wave velocity (a) (4.43 m/s) of the inclusion EI_8 (b) X.XX m/s for other inclusions.

erally separate scatterers like glass beads, titanium oxide and silica carbide are added with the tissue mimicking material. This could alter the elastic properties. In this paper, the objective of the phantom is to mimic different types of tissue elastic properties which are having same echogenicity. So we did not add any separate scatterers. In this work, samples were prepared with agar gel which gives both echogenicity and elastic strength. Hence agar particles might give speckle noise which degrades the image quality which is well seen from all the resultant images. There are a lot of methods in literature to filter out speckle noise. Linear filtering, median filtering and Wiener filtering are some of the speckle reduction methods [31]. In this work, we have used median filtering due to its straight forward implementation which needs only two parameters namely size and shape of the kernel. A kernel of 10×10 pixels was used for filtering process in order to remove the noise. Median filter algorithm replaces a target pixel's value with the median of the neighboring pixels. Number of neighboring pixels is determined by the size and shape of the kernel. Both are selected empirically. Here we have chosen to use 10×10 square kernel to remove speckle noise. The holes in the filtered images were removed by applying min and max filters in order to delineate the boundary of inclusion.

3.5.1. Contrast Transfer Efficiency

The resultant US, UEI and ARFI images are compared in terms of a parameter known as Contrast Transfer Efficiency (CTE). Ponnekanti et al., defined Contrast Transfer Efficiency (CTE) [32] as the ability of any imaging technique to represent the actual modulus ratio in to a reasonable image contrast. It is the performance measure of imaging technique, which quantifies how well the underlying modulus contrast is represented for various categories. Mathematically, it is given by the following expression,

$$CTE = \frac{C_i}{C_m} \tag{4}$$

$$In\ \text{dB}, CTE(\text{dB}) = |C_i(\text{dB})| - |C_m(\text{dB})| \tag{5}$$

where C_i is the observed image contrast from images and C_m is the true modulus contrast (Modulus of inclusion/Modulus of background).

Image contrast is computed as

$$C_i = \frac{S_{bg}}{S_i} \tag{6}$$

where S_i is the mean intensity of pixels inside the inclusion and S_{bg} is the mean intensity of the background pixels.

The procedure for calculating image contrast is explained in Fig. 6(b). The inclusion portion was selected manually and centroid was fixed. From that centroid, Region Of Interest (ROI) of 60×60 pixels was selected, mean intensity was calculated and taken as S_i. From the background, two such ROI of size 40×90 were selected and average intensity was calculated and taken as S_{bg}. The background ROI was selected at the same axial level of the inclusion ROI, to have uniform stress. The size of ROI was chosen to ensure that it covers the maximum part of the portion which is occupied by inclusion and background at the same level of stress. The contrast was calculated by substituting the mean intensities of background and inclusion as per Eq. (6). The image contrast is known as acoustic contrast in ultrasound B-mode, strain contrast in elastogram and displacement contrast in ARFI images. The strain contrast for elastogram of background homogeneous layer was also calculated which is nearer to zero.

The CTE and observed image contrast are plotted against true modulus contrast in Fig. 7. While comparing the trend of observed image contrast of all the three techniques to ideal contrast line shown in Fig. 7(a), we can notice that when true modulus contrast increases from low to high (10–18 dB), Ultrasound B mode shows poor observed image contrast and CTE, where as ARFI and Elastography show improvement. Elastography presents significantly improved CTE for high modulus contrast lesions. Any stiffness imaging method should not over exaggerate and in meanwhile it should not under estimate the underlying tissue modulus contrast. Observed contrast should be such that it atleast approximately reaches the true modulus contrast. Otherwise, it will lead to unnecessary confusions. Hence, we can conclude that both Elastography and ARFI VTTI are efficient in depicting low modulus contrast (less than 10 dB) lesions. For higher modulus ratio, ARFI VTTI presents reasonable displacement contrast whereas Elastography reports exaggerated strain contrast. A plausible explanation for this result is that Elastography uses global external compression which compresses the adjacent area bounded with inclusion which enhances the strain contrast whereas ARFI uses ultrasound pulse to precisely give mechanical excitation to the region of interest.

3.5.2. Lateral image profile

The images are further compared by plotting the lateral image profile; Once the preprocessing of image of size say $m\ X\ n$ was done, the inclusion portion was delineated manually. The centroid of the inclusion was found out. From the centroid, a band of width 20 pixels and length n pixels (covers the image laterally) was selected which is shown in Fig. 6(a). Here 20 pixels have been chosen vertically in image in order to have local uniformity of intensities. In that band, average intensity of pixels in axial direction was computed. The average intensity values were normalized based on

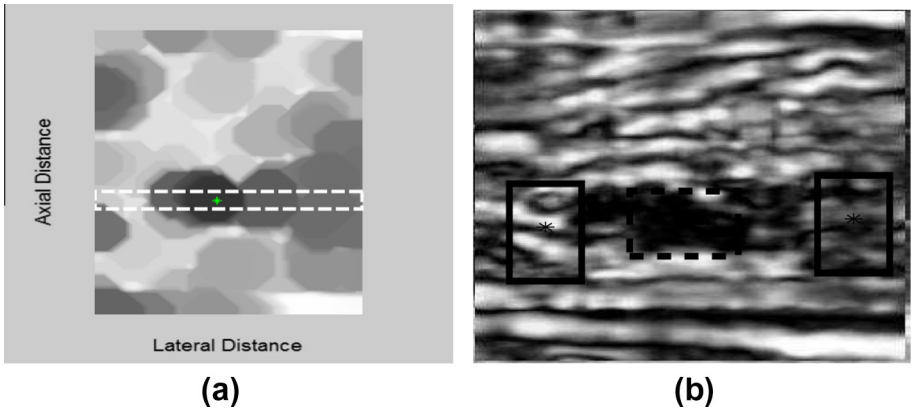

Fig. 6. (a) Band for calculation of lateral profile and (b) calculation of image contrast.

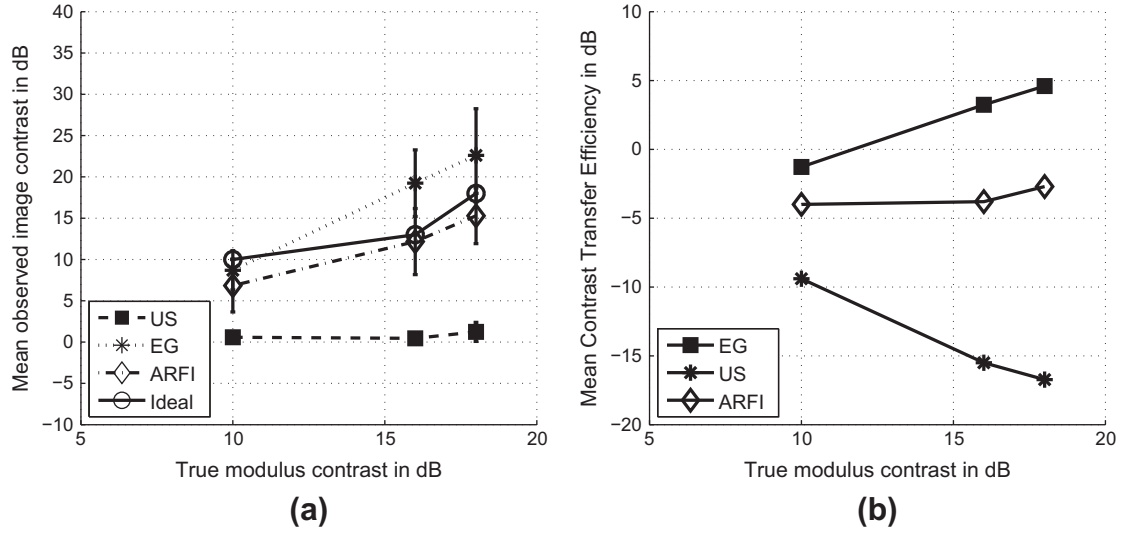

Fig. 7. (a) Observed image contrast for inclusions by conventional B-mode (US), Elastography (EG) and ARFI. (b) Plot of Contrast Transfer Efficiency against true modulus ratio of the prepared inclusions for the three imaging techniques.

maximum intensity and plotted against the lateral distance which is shown in Fig. 8. Strain profile in elastogram is prominent and shows high contrast between background and inclusion than ARFI VTTI and Ultrasound. ARFI VTTI displacement contrast is better than US B-mode and gives reasonable contrast. But in all cases US B mode is poor at representing the contrast.

3.5.3. Clinical validation

We compared the elastic properties of samples with the existing literature [28] and found that they are specifically suitable for mimicking breast and prostate normal and abnormalities (Table 3).

We did clinical validation for Ultrasound Elastography Imaging. The performance results of Elastography were validated with clinical patient images. For this purpose, Ultrasound Elastogram of 30 patients (16 malignant and 14 benign tumors) were collected. The type of lesion of all 30 patients were verified by biopsy. Utrasound B mode (prior to application of force) and elastograms (after compressive force) were acquired using *Siemens Acuson S2000 (Siemens, Erlangen, Germany)* machine at Mediscan Systems, Chennai. Linear array transducer *9L4* with a probe frequency of 8 MHz was used. Fig. 9 shows sample elastogram images of patients which represent the categories of benign and malignant tumors. In clinical setting, the compression applied by radiographer could not be exactly quantified. This might be applicable in Ultrasound Elastography Imaging, since the relative elastic contrast is the property of interest than quantifying the absolute elastic modulus. The relative elastic property is estimated by capturing the pre and post compression echoes.

For clinical images, observed strain contrast was calculated by following the procedure used for phantom images. In clinical elastography, there is no possibility of getting true modulus contrast of underlying lesion. However, Kallel et al. [26] derived an analytic expression which relates true modulus contrast (C_m) and observed strain contrast (C_i) which is stated below.

$$\frac{1}{C_i} = \frac{(1-2v)}{C_m + (1-2v)} + \frac{2}{1 + C_m(3-4v)} \tag{7}$$

where v is the Poisson's ratio of both the inclusion and background. For incompressible materials ($v = 0.5$), the above equation is reduced to

$$C_i = \frac{1 + C_m}{2} \tag{8}$$

The true modulus contrast was calculated for all the 30 cases and observed strain contrast is plotted against the calculated true modulus contrast (Fig. 10(a)). We can notice that benign lesions present low modulus contrast and malignant lesions report high

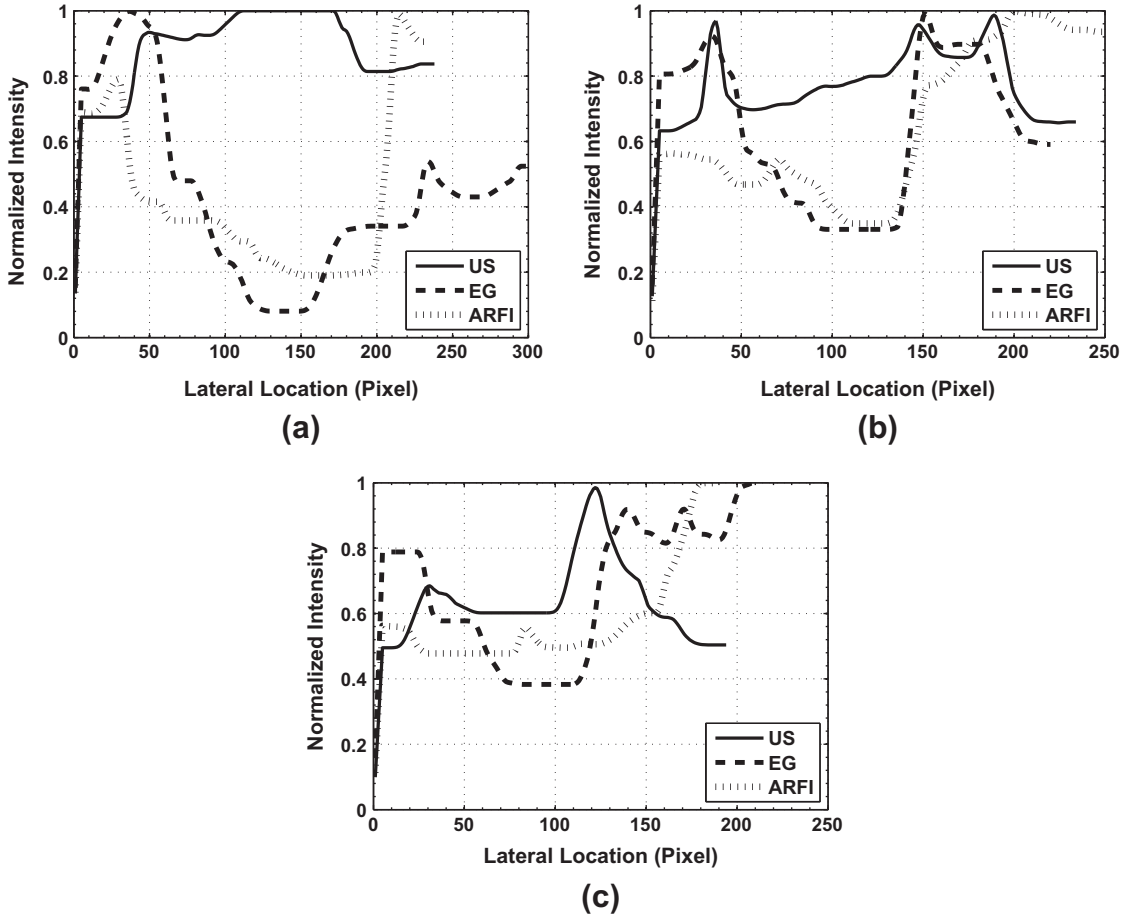

Fig. 8. (a–c) Lateral profile for EI_8, EI_6 and EI_4 inclusions where elastic contrast and displacement contrast are higher than acoustic contrast.

Table 3
Comparison of the elastic moduli of the developed phantoms with those of biological tissues [28].

Phantom Sample	Closely Matching Human Tissue	Elastic Modulus(kPa)
2g	Normal breast & Normal prostate	52±31
4g	Breast Fibrous tissue	182±14
6g & 8g	Breast and prostate Cancerous Tissue	347±75 – 448±10

modulus contrast. Using the elastic contrast, they could be well separated. By investigating the tumor size in elastogram of 30 patients (sample images in Fig. 9), we can notice that benign lesions usually appear either relatively smaller or the same size on sonograms as well as on elastograms where as in case of malignant lesions, the size appears larger on the elastograms. This supports our illustration in phantom images, that high contrast inclusions are expressed with much better large area than low contrast inclusions by Elastography (Section 3.3). The acoustic contrast for all the ultrasound images of 30 patients are calculated and plotted against the estimated elastic contrast in Fig. 10(b). It shows complete decorrelation between the two properties which states that acoustic contrast is completely independent of stiffness of lesions. In addition to that, the acoustic contrast features are overlapped among the two categories of lesions which shows the inability of ultrasound B mode imaging in differentiation of different types of tumors.

Regarding ARFI VTTQ, we have got 4.43 ± 0.35 m/s for only one category EI_8 inclusion. The same value was reported for liver metastases 4.23 ± 0.59 m/s [16] and thyroid papillary carcinoma 4.112 ± 1.413 m/s [15]. For the other categories of inclusions we have got X.XX m/s which means the unmeasurable state of shear wave velocity. Regarding the energy level used in ARFI VTTI and VTTQ (same as that of color Doppler imaging), they result in temperature increase of 0.18 °C and Mechanical Index of 1.9 (admissible range of FDA) which do not pose any risk to patients [12].

Our pilot study on phantoms has some limitations. Four sets of concentration of agar were chosen as representative cancer inclusions and they were investigated. Additional studies with a greater variety of malignant and benign lesions (from 1 to 8 g of agar) in a large series will be required to establish the diagnostic value of UEI and ARFI in terms of their sensitivity and specificity analysis. In this work, we have focused on elasticity variation of different inclusions at same depth. In reality, some categories of cancer lesions may exhibit different echogenicity. The resultant images of tissue mimicking phantoms could be improved by adding separate scatterers like graphite or glass beads in phantom preparation without affecting the stiffness while increasing the echogenicity.

In this study, we can conclude that both ARFI and Elastography imaging improve visualization of unclear inclusions in comparison to fundamental B-scan and ARFI presents almost ideal CTE (due to its region specific compression) where as Elastography enhances the high contrast inclusions (due to global compression). Our study showed that the images of such phantoms could be used as a tool for better understanding of elastographic appearance of different

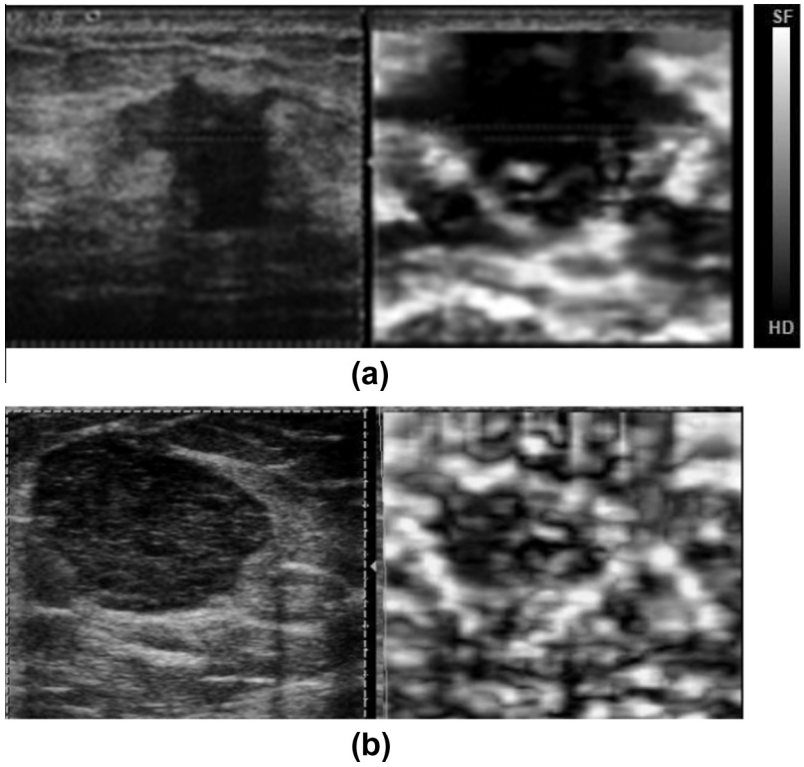

Fig. 9. Clinical elastograms for (a) malignant (b) benign cancer respectively. Left side shows ultrasound and right side shows corresponding elastogram.

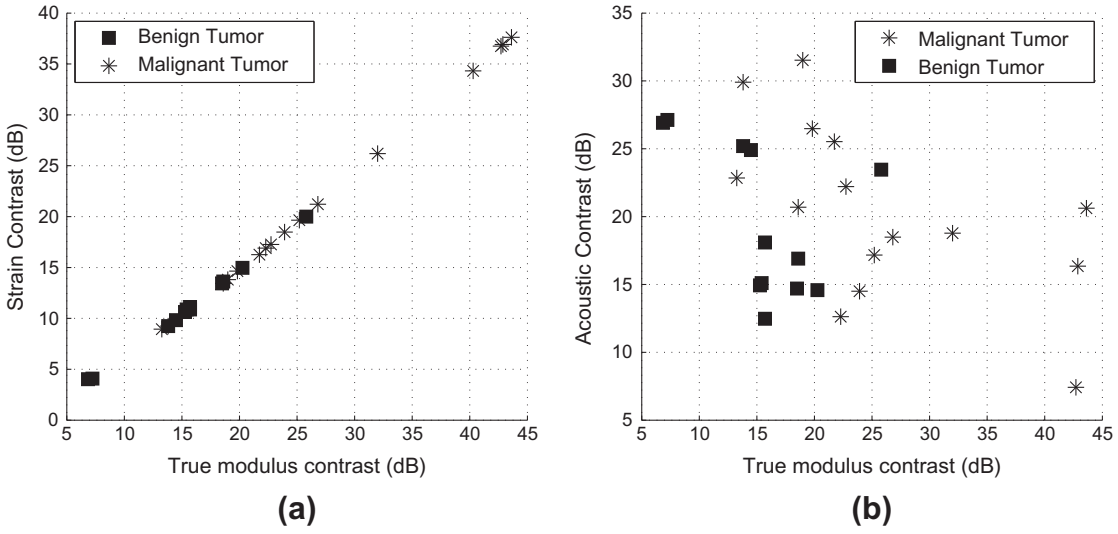

Fig. 10. Observed image contrast versus estimated true modulus contrast for (a) Elastography and (b) ultrasound B mode imaging for clinical patient images.

pathological conditions. In addition to performance analysis of stiffness imaging techniques, it could be even used as calibration tool, training framework to radiographers and laparoscopy training tool in handling graspers. These phantoms could be treated as first order approximation of tissues which allow us to have high level of control on size, depth, modulus ratio, echogenicity and numbers of inclusions present in sot tissue and repeatability in stiffness measurements; otherwise not possible in clinical cases. Moreover the inhomogeneous nature of soft tissue makes the experiments and validation infeasible. Despite phantoms simplify the general complex structure of soft tissue; they are good to test if a method can capture the stiffness properties of a material effectively.

4. Conclusion

The potential usefulness of strain imaging methods like Ultrasound Elastography Imaging and Acoustic Radiation Force Impulse Imaging was investigated for visualization of varying stiffness inclusions. A tissue mimicking phantom was made with embedded inclusions; their acoustical and mechanical properties were obtained. Strain images were taken by UEI and ARFI and they were analyzed in terms of lateral image profile and Contrast Transfer Efficiency. Our investigation shows that the prepared phantoms could be used as a representative model for breast and prostate tissues. In addition to that our study reports that Elastography and

ARFI are efficient in depicting low contrast lesions where as Elastography strongly emphasizes the strain contrast of malignant lesions.

Acknowledgment

The authors would like to thank Dr. Krishnan Balasubramanian and Dr. A. Arockiarajan of IIT Madras for providing the facilities to conduct experiments. Anonymous reviewers are greatly thanked for their very thorough and inspiring review, which substantially improved the manuscript.

References

[1] A.T. Stavros, D. Thickman, C.L. Rapp, M.A. Dennis, S.H. Parker, Solid breast nodules: use of sonography to distinguish between benign and malignant lesions, Radiology 196 (1995) 123–134.
[2] D.M. Parkin, F. Bray, J. Ferlay, P. Pisani, Global cancer statistics, CA Cancer J. Clin. 55 (2005) 74–108.
[3] J. Ophir, Elastography: a quantitative method for imaging the elasticity of biological tissues, Ultrasound Imaging 13 (1991) 111–134.
[4] L. Wilson, D. Robinson, Ultrasonic measurement of small displacements and deformations of tissue, Ultrasound Imaging 4 (1982) 71–82.
[5] R. Dickinson, C. Hill, Measurement of soft tissue motion using correlation between A-scans, Ultrasound Med Biol. 8 (1982) 263–271.
[6] R.M. Lerner, K.J. Parker, J. Holen, R. Gramiak, R.C. Waag, Sono-elasticity: medical elasticity images derived from ultrasound signals in mechanically vibrated targets, Acoust. Imaging 16 (1988) 317–327.
[7] T. Sugimoto, S. Ueha, Itoh, Tissue hardness measurement using the radiation force of focused ultrasound, in: Proc. Ultrasonics Symposium (Honolulu, HI), IEEE, 1990, pp. 1377–1380.
[8] R. Muthupillai, D.J. Lomas, P. Rossman, J.F. Greenleaf, A. Manduca, R.L. Ehman, Magnetic resonance elastography by direct visualization of propagating acoustic strain waves, Science 269 (1995) 1854–1857.
[9] C. Usha Devi, R.M. Vasu, A.K. Sood, Application of ultrasound-tagged photons for measurement of amplitude of vibration of tissue caused by ultrasound: theory, simulation, and experiments, J. Biomed. Opt. 11 (2006).
[10] K. Nightingale, R. Bentley, G. Trahey, Observations of tissue response to acoustic radiation force: opportunities for imaging, Ultrasonic Imaging 24 (2002) 100–108..
[11] K. Nightingale, M. Palmeri, R. Nightingale, G. Trahey, On the feasibility of remote palpation using acoustic radiation force, J. Acoust. Soc. Am. 110 (2001) 625–634.
[12] K. Nightingale, M. Soo, R. Nightingale, G. Trahey, Acoustic radiation force impulse imaging: In vivo demonstration of clinical feasibility, Ultrasound Med. Biol. 28 (2002) 227–235.
[13] B.S. Garra, E.I. Cespedes, J. Ophir, S.R. Pratt, R.A. Zuurbier, C.M. Magnant, M.F. Pennanen, Elastography of breast lesions:initial clinical results, Radiology 202 (1997) 79–86.
[14] A. Lyshchik, T. Higashi, R. Asato, S. Tanaka, J. Ito, JJ. Mai, C. Pellot-Barakat, MF. Insana, AB. Brill, T. Saga, M. Hiraoka, K. Togashi, Thyroid gland tumour diagnosis at us elastography, Radiology 237 (2005) 202–211.
[15] J. Gu, L. Du, M. Bai, H. Chen, X. Jia, J. Zhao, X. Zhang, Preliminary study on the diagnostic value of acoustic radiation force impulse technology for differentiating between benign and malignant thyroid nodules, J. Ultrasound Med. 31 (2012) 763–771.
[16] G. Davies, M. Koenen, Acoustic radiation force impulse elastography in distinguishing hepatic haemangiomata from metastases: preliminary observations, Brit. J. Radiol. 84 (2011) 939–943.
[17] L. Gao, K.J. Parker, R.M. Lerner, S.F. Levinson, Imaging of elastic properties of tissue: a review, Ultrasound Med. Biol. 72 (1996) 959–977.
[18] Thomas L. Szabo, Diagnostic Ultrasound Imaging Inside out, Elesvier Academic Press, 2004.
[19] E. Madsen, R. Zagzebski, Banjavie, P. Jutila, Tissue mimicking materials for ultrasound Phantoms, Am. Assoc. Phys. Med. 5 (1978) 391–394.
[20] E. Madsen, M.A. Hobson, Hairong Shi, T. Varghese, G.R. Frank, Stability of heterogeneous elastography phantoms made from oil dispersions in aqueous gels, Ultrasound Med. Biol. 32 (2003) 261–270.
[21] T.J. Hall, M. Bilgen, M.F. Insana, T.A. Krouskop, Phantom materials for elastogrpahy, IEEE Trans. Ultrason. Ferroelectr. Freq. Control 44 (1997) 1355.
[22] K. Kumar, M.E. Andrews, V. Jayashankar, A.K. Mishra, S. Suresh, Measurement of viscoelastic properties of polyacrylamide-based tissue-mimicking phantoms for Ultrasound Elastography applications, IEEE Trans. Instrum. Meas. 59 (2010) 1224–1232.
[23] L.A. Negron, F. Viola, E.P. Black, C.A. Toth, W.F. Walker, Development and characterization of a vitreous mimicking material for radiation force imaging, IEEE Trans. Ultrason. Ferroelectr. Freq. Control 49 (2002) 1543–1551.
[24] J. Browne, K. Ramnarine, A. Watson, P. Hoskins, Assessment of the acoustic properties of common tissue mimicking test phantoms, Ultrasound Med. Biol. 29 (2003) 1053–1060.
[25] M. Kavitha, M. Ramasubba Reddy, Characterization of tissue mimicking phantoms for acoustic radiation force impulse imaging, in: Proc. Int. Conf. on Imaging Systems and Technology (Manchester, UK), IEEE, 2012, pp. 553–557.
[26] F. Kallel, M. Bertrand, J. Ophir, Fundamental limitations on the contrast-transfer efficiency in elastography: an analytic study, Ultrasound Med. Biol. 22 (1996) 463–470.
[27] Y.C. Fung, Biomechanics: Mechanical Properties of Living Tissues, Springer-Verlog, NewYork, USA, 1993.
[28] T.A. Krouskop, T.M. Wheeler, F. Kallel, B.S. Garra, T.J. Hall, Elastic moduli of breast and prostate tissues under compression, Ultrasound Imaging 20 (1998) 260–274.
[29] G.D. Ludwig, The velocity of sound through tissues and the acoustic impedance of tissues, J. Acoust. Soc. Am. 22 (1950) 862–866.
[30] C.R. Hill, J.C. Bamber, G.R. Haar, Physical Principles of Medical Ultrasonics, John Wiley and Sons, 2004.
[31] V. Oleg, Michailovich, Allen Tannenbaum, Despeckling of medical ultrasound images, IEEE Trans. Ultrason. Ferroelectr. Freq. Control 53 (2006) 64–78.
[32] H. Ponnekanti, J. Ophir, Y. Huang, I. Cespedes, Fundamental mechanical limitations on the visualization of elasticity contrast in elastography, Ultrasound Med. Biol. 21 (1995) 533–543.